Chinese Chemical Letters 34 (2023) 107748

Contents lists available at ScienceDirect

Chinese Chemical Letters

journal homepage: www.elsevier.com/locate/cclet

Effectively arsenic(V) and fluoride removal in geothermal water using magnetic Fe_3O_4@MgO nanoparticles

Qiangying Zhang [a], Xin Tan [a,b], Tao Yu [c,*]

[a] School of Science, Tibet University, Lhasa 850000, China
[b] School of Environmental Science and Engineering, Tianjin University, Tianjin 300350, China
[c] School of Chemical Engineering and Technology, Tianjin University, Tianjin 300350, China

ARTICLE INFO

Article history:
Received 4 June 2022
Revised 25 July 2022
Accepted 12 August 2022
Available online 17 August 2022

Keywords:
Fe_3O_4@MgO adsorbent
Geothermal water
Arsenic(V)
Fluoride
Removal

ABSTRACT

High residual concentration of arsenic and fluoride is a tricky problem to be solved in the process of reinjection after geothermal water utilization. We develop a method to simultaneously remove As(V) and F^- from geothermal water using magnetic Fe_3O_4@MgO adsorbent, fabricated *via* a one-step method. The effects of pH, contact time, adsorbent dose and temperature on the removal efficiency were investigated systematically. The results show that the Fe_3O_4@MgO composite has a wide range of pH (2–11), ultrafast removal dynamics (As(V): 2 min; F^-: 30 min), and high removal efficiency (As(V): 99.9%; F^-: 96.6%). The adsorption kinetics follows the *pseudo*-second-order kinetics model, and the adsorption isotherm model fits Freundlich. The adsorption capacity of As(V) and F^- can reach 123 and 98.4 mg/g, respectively. The exchange of As(V) and F^- with Mg-hydroxyl groups hydrolysis by MgO was determined the adsorption mechanism. The Fe_3O_4@MgO adsorbent was capable of achieving the adsorption efficiency as high as 99.9% for As(V) and 97.3% for F^- in real geothermal water, respectively. Hence, the proposed Fe_3O_4@MgO composite exhibited as an excellent adsorbent for the remediation of As- and F-contaminated geothermal water.

Geothermal resources were regarded as green and renewable energy for development and utilization. Tibet Plateau is the regions of China where high-temperature hydrothermal systems are intensively distributed [1,2]. Arsenic (As) and fluoride (F^-) are two typical high concentration harmful elements in geothermal water. The main resource of As and F^- enrichment in geothermal water mainly comes from rock leaching in geothermal reservoir [3]. In geothermal waters, inorganic As dominated as As(V) due to the gradually oxidized process [4]. The concentration of total As in geothermal water (2.86–5.70 mg/L) has 3 orders of magnitude difference with that in cold water (0.02 mg/L) [5]. Long-term exposure to As-polluted water would result in such severe health problems and cause several diseases such as skin keratinization, neuropathy, vascular injury, and increase the risk of heart disease, even cause skin, liver, lung, and kidney cancer [6]. Therefore, the World Health Organization (WHO) set the concentration levels of As in drinking water as 10 μg/L [7]. Fluoride is often associated with As in geothermal system. An appropriate amount of F^- is beneficial for bone and teeth development and dental health [8]. However, excess uptake of F^- will cause severe health diseases such as osteoporosis, dental, skeletal fluorosis, stiffened and brittle bones [8]. Hence, China has set a more stringently guidance value of 1.0 mg/L for fluoride in drinking water. Consequently, the simultaneous removal of As and F^- from geothermal water is of great significance.

Accordingly, a series of treatment techniques, *e.g.*, electrocoagulation [9], ion-exchange [10], nanofiltration [11], and adsorption [12–14] have been previously investigated for removal of As or F^-. Among these strategies, adsorption technique merits low cost, simplicity and high efficiency [15]. For adsorption, the most important issue is to develop effective adsorbents. Numerous adsorbents have been dedicated for removal of As or F^-, such as MgO [12], Mg/Fe binary hydroxide [16], zirconium alginate [17], mesoporous aluminas [18], granular TiO_2–La adsorbent [19], polymer [20], fiber [21], industrial based adsorbent [22], and metal hydroxide sludge [23]. Among these adsorbents, MgO is inexpensive, non-toxic and limited solubility, which make it an attractive adsorbent for the actual application. Besides, MgO has strong electrostatic attraction towards anions in a wide pH range, due to its high isoelectric point (12.1–12.7) [24]. However, the adsorption capacity for commercial MgO adsorbent is very limited. Thus, continuous improve the adsorption performance of MgO materials is still a big chal-

* Corresponding author.
E-mail address: yutao@tju.edu.cn (T. Yu).

https://doi.org/10.1016/j.cclet.2022.107748
1001-8417/

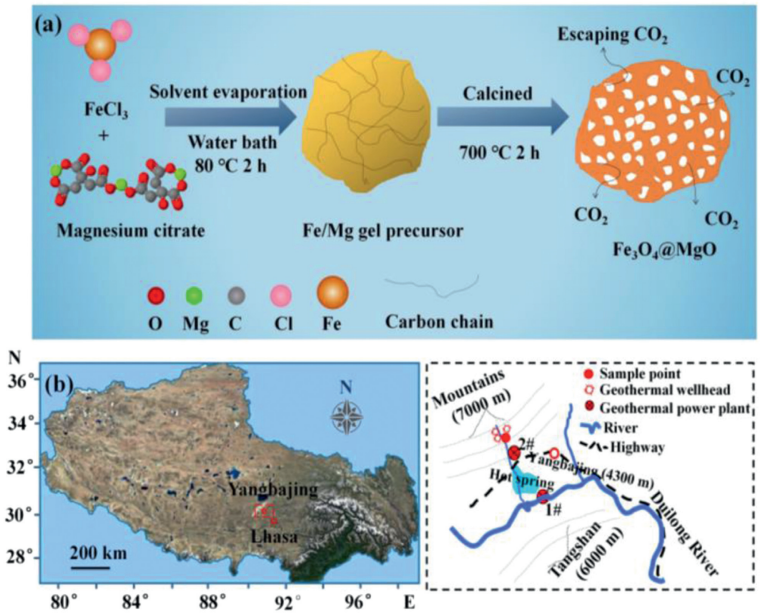

Scheme 1. The synthesis route of Fe_3O_4@MgO composite (a) and the location of sample point (b).

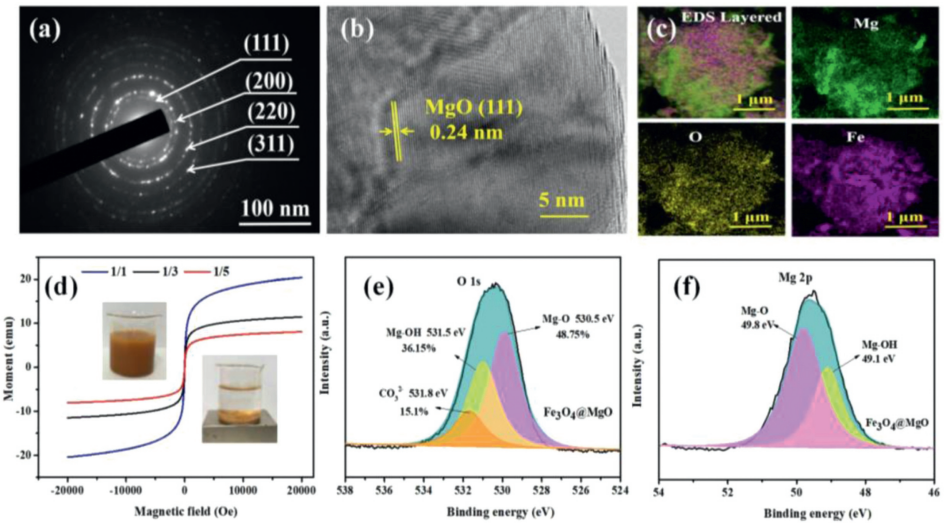

Fig. 1. SAED pattern (a), HR-TEM image (b), elemental mapping for Mg, Fe and O (c), magnetization curves (d), high-resolution O 1s (e) and Mg 2p (f) spectra of the as-synthesized composites.

lenge. Much effort has been carried out to fabricate MgO adsorbents to remove F^- [25,26], and few adsorbents are available for simultaneous removal of As and F^-. Thus, it is still a challenge to develop effective and environmentally friendly adsorbents with superior adsorption capacities for removing both As and F^- simultaneously.

Therefore, the main objectives of this research were to develop a simple procedure to prepare magnetic MgO composite adsorbent by one-step pyrolysis (Scheme 1a) for effective As(V) and F^- removal, characterize the adsorbent, and finally evaluate its As(V) and F^- adsorption efficiencies and capacities, examine the influence of co-existing anions, aiming to apply it to the real geothermal water for As(V) and F^- removal. As the location of sample point presented in Scheme 1b, the geothermal water was collected from Yangbajing in Lhasa City, Tibet.

The main reagents, fabrication and characterization of Fe_3O_4@MgO adsorbent, adsorption experiments are exhibited in the Supporting information. As the result of SAED pattern in Fig. 1a, bright circled rings were clearly observed, corresponding to the spacing of (111), (200), (220) and (311) planes for MgO. As demonstrated in the HR-TEM image (Fig. 1b), a lattice fringes was clearly identified and the spacing is matching with the (111) planes of MgO, which are in accordance with the following XRD results. The results of elemental mapping in Fig. 1c shown that the distribution of Fe, Mg and O was uniform. Moreover, the magnetic behavior of the synthesized composites were measured by hysteresis loops. The near-zero coercivity and remanence according to the magnetization curves (Fig. 1d) demonstrated that the synthesized composites are superparamagnetic. The corresponding saturation magnetization strengths are 20.45, 11.45 and 8.06 emu/g, respectively. Clearly, a transparent solution can be obtained after separation by a magnet within 5 min, and the photographs of the solution before and after separation are shown for the illustration. For high-resolution O 1s and Mg 2p spectra analysis in Figs. 1e and f, 530.5 (49.8), 531.5 (49.1) and 531.8 eV correspond to the peaks of Mg-O, Mg-OH and CO_3^{2-} respectively

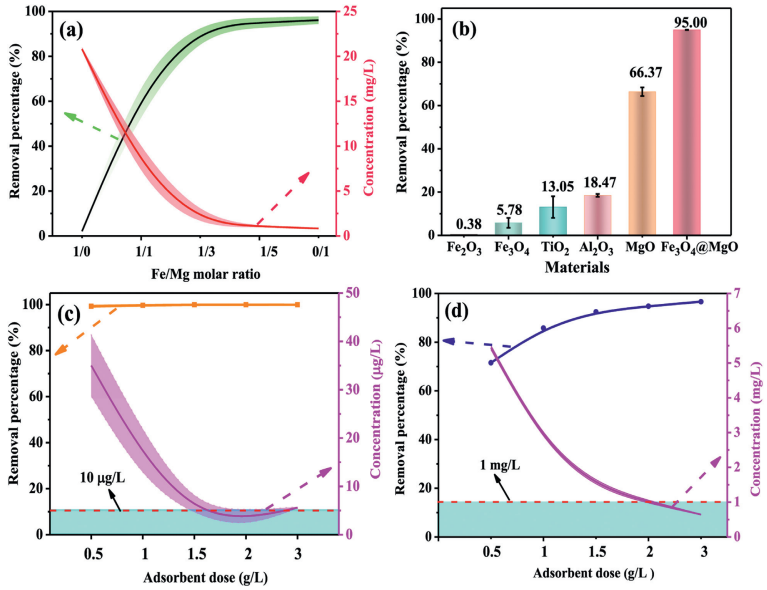

Fig. 2. (a) F^- removal by synthesized composites as a function of Fe/Mg ratio. (b) Comparison of F^- removal efficiency for different adsorbents. As(V) (c) and F^- (d) removal by Fe_3O_4@MgO as a function of adsorbent dose.

[12], which indicates that Mg–OH and $MgCO_3$ are formed by hydrolysis of Fe_3O_4@MgO. Moreover, the TEM and SEM images, EDX analysis and S_{BET} for the as-synthesized magnetic composites were displayed in Fig. S1 and Table S1 (Supporting information).

The F^- removal efficiencies on the composites were evaluated. As the results depicted in Fig. 2a, as the molar ratio of Fe/Mg was decreased to 1/5, the removal efficiency was remarkable increased to that of pure MgO. Meanwhile, the residual F^- concentration was below 1 mg/L, thus the molar ratio of Fe/Mg as 1/5 was employed for subsequent fabrication process. Additionally, magnesium citrate has a long carbon chain, which will be decomposed into CO_2 with the increase of pyrolysis temperature, and formation abundant pores by escaping CO_2. The effect of pyrolysis temperature on F^- removal performance was depicted in Fig. S2 (Supporting information). The pyrolysis temperature has little effect on the removal performance. In order to preliminarily evaluate the defluoridation efficiency of the adsorbents, the as-synthesized composite was compared with the conventional oxides (Fe_2O_3, Fe_3O_4, Al_2O_3, TiO_2 and MgO). As illustrated in Fig. 2b. Attractively, the as-synthesized composite presented a marked defluoridation efficiency of 95%, which is much higher than synthesized adsorbents [27–29]. Meanwhile, the initial concentration of F^- (20 mg/L) is higher in this work. Also, the effect of adsorbent dose on As and F^- removal was investigated, and the results are shown in Figs. 2c and d. The removal efficiency for As reaches 100% in the whole dose from 0.5 g/L to 3 g/L. The residual As was decreased to below 10 μg/L as the dose higher than 1.5 g/L. Significantly, the residual F^- dramatically reduced from 5.5 mg/L to 0.65 mg/L as dose increased from 0.5 g/L to 3.0 g/L. Attributed to the abundant available reaction sites as the adsorbent dose increase. Hence, the optimum adsorbent dose was maintained as 3 g/L.

Solution pH will not only affect the charge forms on the surface of adsorbent, but also affect the existences of target ions. Hence, the effect of pH on As(V) and F^- removal was investigated, and the results are illustrated in Fig. 3a. In general, As species in the geothermal water mainly exists in the form of As(V), due to the oxidation [30], and As(V) were dominated as H_3AsO_4 (pKa_1 2.20, pKa_2 6.93, pKa_3 11.53). The pH in geothermal water was 9.02. Hence, the As(V) specie was dominated as $HAsO_4^{2-}$. For arsenic species adsorption, both As(III) and As(V) were studied, compared to As(V), the removal efficiency for As(III) in Fig. S3 (Supporting information) has a relatively narrow adsorption pH range (2–10), and low removal rate (91.5%) due to the electrical neutrality of As(III). The as-prepared adsorbent has high removal efficiency for both As(III) and As(V), and a better affinity for As(V). Considering that the geothermal water mainly exists in the form of As(V), therefore, As(V) was chosen as the target ion to investigate the adsorption performance of arsenic. The removal efficiency for As(V) is nearly 100% in the pH range of 2-12, the F^- removal efficiency dramatically reduced to 56% at pH 12. Surprisingly, As(V) and F^- adsorption by Fe_3O_4@MgO is less sensitive to pH (2-11), due to the high isoelectric point (pH_{PZC}) of Fe_3O_4@MgO adsorbent (12.8). At pH < pH_{PZC}, the surface of adsorbents is positively charged, and attracts the negatively charged target ions, thus maintaining high removal efficiency. While pH > pH_{PZC}, the surface of the adsorbent tends to be negative charged and occurs as repulsion interaction, resulting in a reduction in removal efficiency. The prepared adsorbent merits a wide pH range (2-11). Due to the heat transfer with the environment, it is necessary to investigate the influence of temperature. As results presented in Fig. 3b. Obviously, the F^- removal efficiency increased significantly with increasing temperature from 20 °C to 40 °C, followed by a plateau. Similarly, the results for As(V) adsorption were consistent with F^-, whereas its removal efficiency has been maintained up to 99.3%–99.9%. The similar results were also observed by using magnetite-reduced graphene oxide for As removal [31]. Comparatively, the adsorption efficiency of F^- is more obvious than that of As(V), due to the high initial concentration of F^- (20 mg/L). The equilibrium time can reflect the kinetics of the adsorbent for target ions. The effect of contact time on As(V) and F^- removal are depicted in Fig. 3c. The magnetic composite shows a ultrafast dynamics for As(V), approximately 96% removal efficiency was achieved within 2 min, and almost 99.9% was removed within 10 min. Initially, an markedly increase in removal efficiency for F^- was observed with the contact time increased to 30 min, and the residual F^- dramatically reduced to 1 mg/L as contact time increased to 120 min. In order to ensure higher removal rate, 180 min was selected for subsequent process. Moreover, the proposed adsorbent has fast kinetics for As(V) and F^- than other MgO adsorbents [12,32-34], and has highly feasible in practical application.

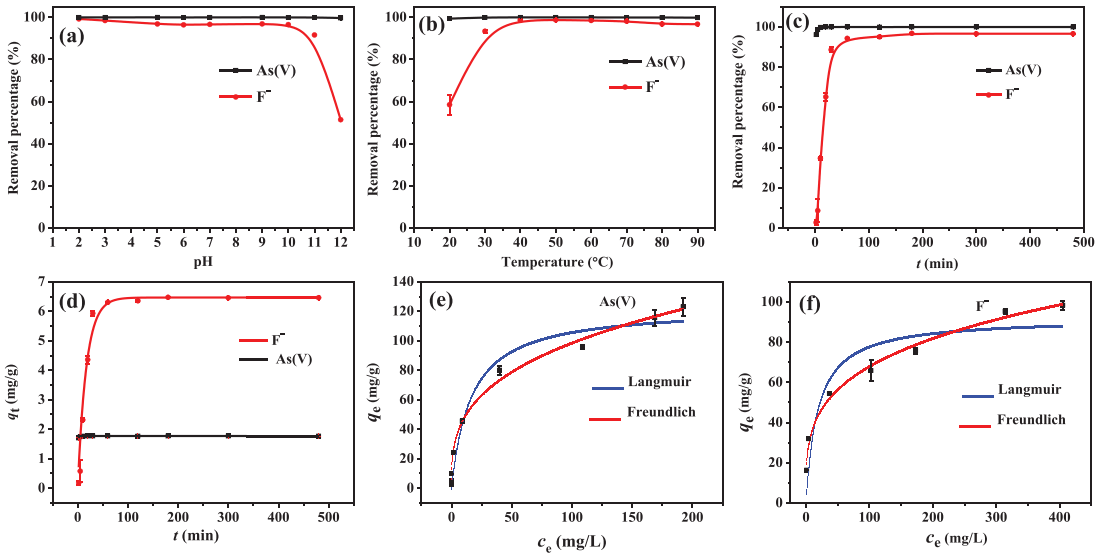

Fig. 3. As(V) and F^- removal by Fe_3O_4@MgO as a function of initial pH (a), temperature (b) and contact time (c); the pseudo-second order model (d); the adsorption isotherm for As(V) (e) and F^- (f).

The adsorption kinetic process of As(V) and F^- onto Fe_3O_4@MgO were investigated by using pseudo-first-order and pseudo-second-order kinetic models [35]. As observed, the experimental data were well-correlated with the pseudo-second-order model, and the non-linear fitting curves are depicted in Fig. 3d along with the relevant kinetics parameters listed in Table S2 (Supporting information). It indicates that As(V) and F^- adsorption on Fe_3O_4@MgO was rapid and controlled by chemical adsorption, which follows the second-order kinetic model. The adsorption isotherms of As(V) and F^- on Fe_3O_4@MgO were investigated. Two commonly used isotherm models (Langmuir and Freundlich) are employed for data analysis [35], and the results are depicted in Figs. 3e and f along with the corresponding parameters in Table S3 (Supporting information). The adsorption behavior of As(V) is consistent with both Langmuir and Freundlich models, while the Freundlich model was more suitable for As(V) adsorption with a higher correlation coefficient value of 0.994. For F^- adsorption, the Freundlich model gives a better fit to the experimental data with a correlation coefficient value of 0.989. The similar result was consistent with the previously reported MgO adsorbent [32]. Also, adsorption capacity is an important parameter for evaluating the capacity of active sites on the synthesized adsorbent. As the result presented in Fig. S4 (Supporting information), an increase in adsorption capacity was observed with the initial concentration. The adsorption capacity of the synthesized adsorbent for As(V) and F^- was calculated to be as high as 123 ± 6 mg/g and 98.4 ± 2.23 mg/g, respectively. A comparison of adsorption capacity on different adsorbents was presented in Table S4 (Supporting information). The adsorption capacities of As(V) and F^- obtained with the synthesized Fe_3O_4@MgO adsorbent was much higher than those obtained with previously reported metal oxide adsorbent [13,14,16,19,20], suggesting that the magnetic pores structures MgO prepared here are highly efficient potential materials for removing As(V) and F^- from aqueous solution.

In geothermal water, many anions often coexist with target ions and have a competitive adsorption. The removal efficiencies of As(V) and F^- by common coexisting anions (HCO_3^-, SO_4^{2-}, Cl^-, CO_3^{2-}, SiO_3^{2-}, PO_4^{3-} and NO_3^-) at 0.1, 1 and 10 mmol/L were investigated. As presented in Figs. 4a and b, NO_3^-, Cl^-, HCO_3^-, CO_3^{2-} and SO_4^{2-} posed negligible effect on As(V) and F^- adsorption in the whole concentration range of 0.1-10 mmol/L. However, a significant interference was observed on As(V) and F^- adsorption by SiO_3^{2-} and PO_4^{3-} ions when the concentration above 10 mmol/L. The observed obviously reduction in adsorption of As(V) and F^- attributed to the presence of SiO_3^{2-} and PO_4^{3-} ions competition for active sites, and the coexisting anions was in the order of PO_4^{3-} > SiO_3^{2-} > (HCO_3^-, SO_4^{2-}, Cl^-, CO_3^{2-} and NO_3^-). The as-prepared adsorbent has a good anti-interference ability and can meet the requirements of real geothermal water analysis.

For reveal the adsorption mechanism, X-ray diffraction (XRD) were conducted, as the patterns shown in Fig. 4c. In the XRD pattern of pure MgO, 2θ degree at 36.9°, 42.9°, 62.3°, 74.7° and 78.6° were ascribed to the (111), (200), (220), (311) and (222) planes of MgO (JCPDS No. 45-0946). Compare to $FeCl_3$ added, new peaks appeared at 2θ degree of 30.1°, 35.4°, 53.4° and 57.0°, which indexed to the (220), (311), (422) and (511) planes of the Fe_3O_4 (JCPDS No. 19-0629), indicating that the Fe_3O_4@MgO composite was successfully prepared. As expected, the hydrolyzed Fe_3O_4@MgO was obtained new peaks (1-6), corresponded to (001), (101), (102), (110), (220) and (201) planes of $Mg(OH)_2$ (JCPDS No. 44-1482), demonstrates that $Mg(OH)_2$ was generated through hydrolysis progress. After adsorption As(V) and F^-, the peak of $Mg(OH)_2$ was slightly weakened. Besides, the FT-IR was employed to investigated the function groups of magnetic composites before and after As(V) and F^- adsorption. As presented in Fig. 4d, the FT-IR spectra of Fe_3O_4@MgO exhibit a wide and strong band at 3440 cm^{-1} and a relative week band at 1645 cm^{-1}, which are assigned to the stretching vibration modes of −OH bands and the bending vibration of H−O−H band, respectively [36]. The peak observed at 1489 cm^{-1} was ascribed to the asymmetric stretching vibration of carbonates, the carbonates are mainly derived from the combination of MgO and CO_2 in the air [24], which is further confirmed by the following XPS analysis. The band observed at 561 cm^{-1} and 434 cm^{-1} were corresponded to the Fe−O−Fe and Mg−O stretching vibration, respectively. The $Mg(OH)_2$ was generated after immersing Fe_3O_4@MgO into deionized water, a new strong and sharp diffraction peak appears at 3689 cm^{-1}, which is assigned to the stretching vibration of –OH groups in $Mg(OH)_2$, indicating that –OH groups are generated from the hydrolysis process. After adsorption As(V), a new brand for the As-O stretching vibration at 853 cm^{-1} was formed. Due to the peak of F-Mg around at 530 cm^{-1} was overlapped with that of Fe−O−Fe (561 cm^{-1}).

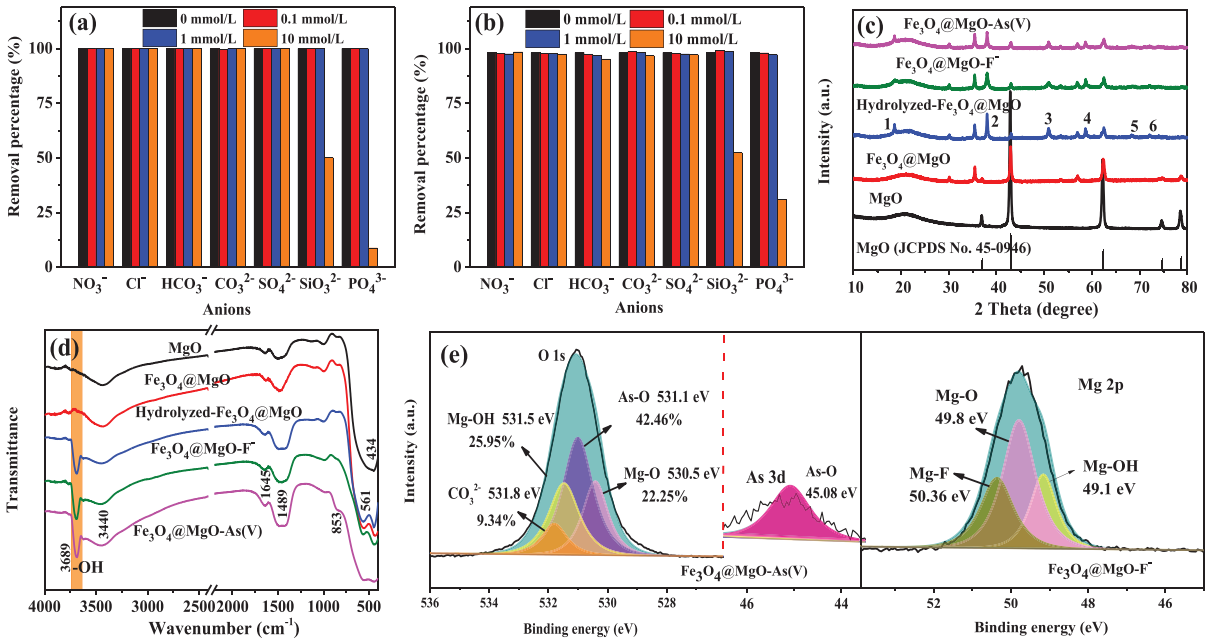

Fig. 4. The effect of competing anions for As(V) (a) and F^- (b) removal, XRD pattern (c), FT-IR spectra (d), high-resolution O 1s, As 3d and Mg 2p (e) spectra of the as-synthesized composites.

The IR spectra showed that the –OH groups are generated from the magnetic composites through hydrolysis process, and then exchanged with As(V) and F^-. For further explore adsorption mechanism, the Fe_3O_4@MgO composite before and after As(V) and F adsorption were characterized by XPS analysis. As presented the high-resolution As 3d and F 1s spectra in Fig. S5 (Supporting information), the binding energies of the adsorbent show peaks of As 3d and F 1s at 45.08 eV and 684.87 eV, respectively, indicating that F and As(V) were bound to the surface. As presented the high resolution O 1s, Mg 2p and As 3d peaks analysis after As(V) and F adsorption in Fig. 4e, the As–O peak appeared at 531.1eV and the intensity of Mg–OH decreased, indicating that As exchanged with hydroxyl groups in Mg–OH. Also, the Mg-F peaks appeared at 50.36 eV after F^- adsorption, indicating the exchange with Mg–OH. Based on the characterization results of XRD, FT-IR and XPS, the adsorption mechanism of the material was demonstrated as follows (Eqs. 1-6):

$$MgO + H_2O \rightarrow Mg(OH)_2 \quad (1)$$

$$MgO + CO_2 \rightarrow MgCO_3 \quad (2)$$

$$Mg(OH)_2 + F^- \rightarrow Mg(OH)F + OH^- \quad (3)$$

$$MgCO_3 + 2F^- \rightarrow MgF_2 + {CO_3}^{2-} \quad (4)$$

$$Mg(OH)_2 + {HAsO_4}^{2-} \rightarrow MgAsO_4 + H_2O \quad (5)$$

$$MgCO_3 + {HAsO_4}^{2-} \rightarrow MgHAsO_4 + {CO_3}^{2-} \quad (6)$$

Under the optimum conditions, the removal efficiency of the as-prepared adsorbent on real geothermal water was investigated. The conventional parameters and major cations and anions of geothermal water are presented in Table S5 (Supporting information). The hydrochemical types of geothermal water were Na–HCO_3 and Na–Cl. As shown in Fig. S6 (Supporting information), the initial concentrations of total As and F^- in geothermal water are as high as 3.14 and 12.95 mg/L, respectively. After adding 90 mg adsorbent to 30 mL geothermal water, the removal efficiency can achieve 99.9% and 97.3% for total As and F^-. The residual total As and F^- concentrations were 4.4 μg/L and 0.35 mg/L, respectively. The regeneration of the as-prepared magnetic composite was further investigated, the reusability in Fig. S7 (Supporting information) revealed that the removal efficiency was still above 80% after three adsorption-regeneration cycles. Furthermore, the dissolution of Fe_3O_4@MgO adsorbent has been studied, and the results indicated that less than 0.085% of MgO have dissolved during the adsorption process. The established process is highly feasible for the remediation of As- and F-contaminated geothermal water.

In this paper, a superior adsorbent, Fe_3O_4@MgO was prepared and examined for its potential to simultaneous removal of As(V) and F^- from geothermal water system. Firstly, the lab-scale conditional experiments were initially performed to investigate the effects of different parameters on removal efficiency. The established adsorption process mainly involves the exchange of As(V) and F^- with Mg-hydroxyl groups hydrolysis from MgO. The obtained adsorbent features an excellent magnetic separation ability, high removal efficiency, ultrafast removal dynamics and a super wide pH range. It is demonstrated that Fe_3O_4@MgO adsorbent has superior performance for the remediation of high concentration As- and F-contaminated geothermal water.

Declaration of competing interest

The authors declare that they have no known competing financial interests or personal relationships that could have appeared to influence the work reported in this paper.

Acknowledgments

This research was funded by the Second Comprehensive Scientific Investigation Project of Qinghai-Tibet Plateau (No. 2019QZKK0603), the National Natural Science Foundation of China (No. 22066022), Science and Technology Plan Projects of Tibet Autonomous Region (No. ZYYD2022000255), Key Projects of "Science

and Technology Help Economy 2020" (No. SQ2020YFF0423891), Key Projects of Solid Waste Recycling (No. 2019YFC1904103-04).

Supplementary materials

Supplementary material associated with this article can be found, in the online version, at doi:10.1016/j.cclet.2022.107748.

References

[1] Q.H. Guo, Appl. Geochem. 27 (2012) 1887–1898.
[2] Q.H. Guo, Y.W. Cao, J.X. Li, X.B. Zhang, Y.X. Wang, Appl. Geochem. 62 (2015) 164–170.
[3] Z. Jiang, P. Li, J. Tu, et al., Int. Biodeterior. Biodegrad. 128 (2018) 28–35.
[4] J. Bundschuh, J.P. Maity, B. Nath, et al., J. Hazard Mater. 262 (2013) 951–959.
[5] Q.H. Guo, Y. Wang, W. Liu, J. Volcanol, Geoth. Res. 166 (2007) 255–268.
[6] D. Mohan, C.U. Pittman, J. Hazard Mater. 142 (2007) 1–53.
[7] S.R. Kanel, J.M. Grenèche, H. Choi, Environ. Sci. Technol. 40 (2006) 2045–2050.
[8] A. Ghosh, K. Mukherjee, S.K. Ghosh, B. Saha, Res. Chem. Intermed. 39 (2012) 2881–2915.
[9] L.S. Thakur, P. Mondal, J. Environ. Manag. 190 (2017) 102–112.
[10] B. An, Q. Liang, D. Zhao, Water Res. 45 (2011) 1961–1972.
[11] A.P. Padilla, H. Saitua, Desalination 257 (2010) 16–21.
[12] P.P. Gao, X.K. Tian, C. Yang, et al., Environ. Sci.: Nano 3 (2016) 1416–1424.
[13] C. Jing, J. Cui, Y. Huang, A. Li, ACS Appl. Mater. Interfaces 4 (2012) 714–720.
[14] S.M. Prabhu, P. Koilraj, K. Sasaki, Chem. Eng. J. 325 (2017) 1–13.
[15] X. Zhang, M. Wu, H. Dong, H. Li, B. Pan, Environ. Sci. Technol. 51 (2017) 6326–6334.
[16] D. Kang, X. Yu, S. Tong, et al., Chem. Eng. J. 228 (2013) 731–740.
[17] T. Yu, Y.L. Chen, Y.Z. Zhang, et al., Chin. Chem. Lett. 32 (2021) 3410–3415.
[18] W. Li, C.Y. Cao, L.Y. Wu, M.F. Ge, W.G. Song, J. Hazard Mater. 198 (2011) 143–150.
[19] L. Yan, H. Tu, T. Chan, C. Jing, Chem. Eng. J. 313 (2017) 983–992.
[20] V. Kumar, N. Talreja, D. Deva, et al., Desalination 282 (2011) 27–38.
[21] Y. Meng, J.N Wang, C. Cheng, X. Yang, A.M. Li, Chin. Chem. Lett. 23 (2012) 863–866.
[22] S. Bibi, A. Farooqi, K. Hussain, N. Haider, J. Clean. Prod. 87 (2015) 882–896.
[23] C. García-Gómez, M.L. Rivera-Huerta, F. Almazán-García, et al., Water, Air, Soil Pollut. 227 (2016) 1–16.
[24] Z. Jin, Y. Jia, K.S. Zhang, et al., J. Alloys Compd. 675 (2016) 292–300.
[25] L.X. Li, D. Xu, X.Q. Li, W.C. Liu, Y. Jia, New J. Chem. 38 (2014) 5445–5452.
[26] Z. Jin, Y. Jia, T. Luo, et al., Appl. Surf. Sci. 357 (2015) 1080–1088.
[27] A. Dhillon, S.K. Soni, D. Kumar, J. Fluorine Chem. 199 (2017) 67–76.
[28] G.Zhang D.Tang, Chem. Eng. J. 283 (2016) 721–729.
[29] L. Chai, Y. Wang, N. Zhao, W. Yang, X. You, Water Res. 47 (2013) 4040–4049.
[30] T.F. Lin, J.K. Wu, Water Res. 35 (2001) 2049–2057.
[31] V. Chandra, J. Park, Y. Chun, et al., ACS Nano 4 (2010) 3979–3986.
[32] K. Zhang, S. Wu, X. Wang, et al., J. Colloid Interface Sci. 446 (2015) 194–202.
[33] N.A. Oladoja, S. Chen, J.E. Drewes, B. Helmreich, Chem. Eng. J. 281 (2015) 632–643.
[34] N.A. Oladoja, S. Hu, J.E. Drewes, B. Helmreich, Sep. Purif. Technol. 162 (2016) 195–202.
[35] Y. Wei, H. Liu, C. Liu, et al., Water Res. 150 (2019) 182–190.
[36] Q.Y. Zhang, M. He, B.B. Chen, B. Hu, ACS Omega 3 (2018) 3752–3759.